



OPEN

Contact stiffness of randomly rough surfaces

SUBJECT AREAS:

MECHANICAL
ENGINEERING

ELECTRICAL AND ELECTRONIC
ENGINEERING

APPLIED PHYSICS

SURFACES, INTERFACES AND
THIN FILMS

Roman Pohrt & Valentin L. Popov

Technische Universität Berlin, Sekr. C8-4, Str. des 17. Juni 135, 10623 Berlin, Germany.

Received
15 May 2013

Accepted
1 November 2013

Published
21 November 2013

Correspondence and
requests for materials
should be addressed to
R.P. (roman.pohrt@tu-
berlin.de)

We investigate the contact stiffness of an elastic half-space and a rigid indenter with randomly rough surface having a power spectrum $C_{2D}(q) \propto q^{-2H-2}$, where q is the wave vector. The range of $H \in (-1, 3)$ is studied covering a wide range of roughness types from white noise to smooth single asperities. At low forces, the contact stiffness is in all cases a power law function of the normal force with an exponent α . For $H > 2$, the simple Hertzian behavior is observed ($\alpha = 1/3$). In the range of $0 < H < 2$, the Pohrt-Popov behavior is valid ($\alpha = 1/(1+H)$). For $H < 0$, a power law with a constant power of approximately 0.9 is observed, while the exact value depends on the number of modes used to produce the rough surface. Interpretation of the three regions is given both in the frame of the three dimensional contact mechanics and the method of dimensionality reduction (MDR). The influence of the long wavelength roll-off is investigated and discussed.

Surface roughness has a major influence on many physical phenomena in contacts such as friction, wear, sealing, adhesion, as well as electrical and thermal conductivity¹. Bowden and Tabor² were first to point out that the real contact area between two bodies is typically orders of magnitude smaller than the apparent contact area. In the 1950's and 60's many studies were inspired by these findings, including basic contributions by Archard³ and Greenwood and Williamson⁴. In the last years, an emphasis was made on calculation of the real contact area in the contact of fractal, self-affine surfaces, showing roughness in a wide range of wave vectors^{5,6}.

In the present paper, we investigate the contact stiffness of rough contacts. Contact stiffness is one of the key quantities in the contact mechanics of elastic bodies⁷. It can easily be deduced from experiments and has exact analytical proportionality to the lateral stiffness⁸ as well as the thermal and electrical interfacial conductivity⁹⁻¹¹. Therefore in the past, the contact stiffness has been investigated using numerical methods⁶ as well as in the frame of different contact theories.

We consider self-affine surfaces with the power spectral density being a power-law function of the wave vector q :

$$C_{2D}(q) \propto q^{-2H-2}. \quad (1)$$

In the range of $0 < H < 1$, an equivalent fractal dimension ranging from 2 to 3 can be associated with these surfaces:

$$D_f = 3 - H. \quad (2)$$

Self-affine surfaces are often investigated in this particular range, but eq. (1) does not naturally impose such a restriction. We numerically generated surfaces with H from -1 to 3 and solved the three-dimensional contact problem for a wide range of normal forces F_N . At low forces, the contact stiffness k was found to rise with the force according to a power law

$$k = \frac{\partial F_N}{\partial d} \propto F_N^\alpha, \quad (3)$$

where d is the indentation depth and α a constant power. The result (3) is an issue of contemporary controversial discussion. The Greenwood and Williamson model⁴ predicts for the contact stiffness approximate proportionality to the normal force

$$k \approx \frac{F_N}{h} \quad (4)$$

where h is the rms roughness of the surface:



$$\langle h^2 \rangle \propto \int_{q_{\min}}^{q_{\max}} q^{-2H-2} q dq, \quad (5)$$

q_{\min} and q_{\max} are the minimum and the maximum wave vectors in the power spectrum. Paggi and Barber¹¹ found $\alpha \approx 0.82$ for $H = 0.7$, Ciavarella et. al. find the exponent 0.6¹⁰, Pohrt and Popov¹² reported results of boundary element simulations giving α in the interval from 0.51 to 0.77 for H varying from 1 to 0. Later, they presented analytical arguments showing that

$$\alpha = \frac{1}{H+1} \quad (6)$$

in the interval $H \in (0, 1)^{13}$.

We will show that the main part of controversy may be due to the fact that the power α is a function of the parameter H . Depending on the character of the roughness, all values of α between 1/3 and 1 can be observed.

Results

We considered a rigid flat indenter superimposed with a roughness produced using the spectral power density (1). The indenter was pressed into an elastic half-space, and the dependence of the contact stiffness on the indentation depth was determined numerically using the 3D boundary element method (BEM). In each case, the contact stiffness at low forces was found to rise with the force according to a power law (3). The dependency of the exponent α on the Hurst exponent is shown in Fig. 1 (gray dashed lines). Three regions with qualitatively different behavior can be identified. For $H < 0$ the exponent α is almost constant but depends on the grid size used. For $0 < H < 2$, α decreases and follows accurately the thin black line of the Pohrt/Popov relation^{13,14} $\alpha = (H+1)^{-1}$. For values of H greater than 2, the exponent α remains approximately constant and equal to 1/3.

In¹³, it was shown that for $0 < H < 1$ the contact stiffness of rough surfaces can be described using the method of dimensionality reduction (MDR)^{20,21}. In this paper we used the same procedure as in¹³ but extended the studied region to $-1 < H < 3$. The results obtained with the MDR are shown in Fig. 1 by blue lines. The qualitative behavior obtained with both BEM and MDR is the same. Only in the region $H < 0$, the dependence is slightly different. Note that the results presented in Fig. 1 refer to roughness having no long wavelength cut-off or roll-off. This means that the power dependence (1) of spectral density was valid for all wave vectors up to the diameter of the indenter.

Many technical surfaces do not show the fractal behavior described by the spectrum (1) for all wave vectors. For macroscopic surfaces, the relation of the type (1) is typically valid up to some characteristic wave vector q_0 . For smaller wave vectors the spectral density does not increase any more according to (1) but rather remains approximately constant or even goes down. For simplicity, one often assumes that the power spectrum has either the long wavelength “roll-off”:

$$C_{2D}(q) = \text{const} \cdot \begin{cases} q^{-2H-2}, & q > q_0 \\ q_0^{-2H-2}, & \text{otherwise} \end{cases} \quad (7)$$

or the long wave length “cut-off”:

$$C_{2D}(q) = \text{const} \cdot \begin{cases} q^{-2H-2}, & q > q_0 \\ 0, & \text{otherwise} \end{cases}. \quad (8)$$

For fractal rough surfaces including a roll-off, the dependence of the normal contact stiffness on normal force is shown in Fig. 2(a). It was found to first rise in a power-law-fashion (3) with a later cross-over to an almost linear dependence, see Fig. 2 (a).

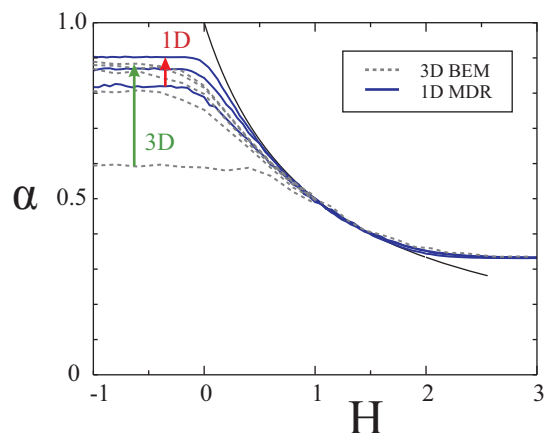


Figure 1 | Dependency of the power α in the force-stiffness-relation (3) on H . The gray dashed lines are results of a 3D Boundary Element study. The blue bold lines are obtained using the 1D method of dimensionality reduction. The following grid sizes were used (following the arrows): $N_{3D} = \{2^7; 2^8; 2^9; 2^{10}\}$ in BEM calculations and $N_{1D} = \{2^9; 2^{11}; 2^{15}\}$ in MDR calculations. For values $H < 0$, α is found to be a function of the grid size N in both 3D and 1D simulations, but it appears independent of H , see eq. (24). Values of $H > 2$ lead to $\alpha = 1/3$, corresponding to the Hertzian behavior. In the intermediate region of approximately $0 < H < 2$, the Pohrt/Popov-relation (fine black line) $\alpha = (H+1)^{-1}$ applies^{13,14}.

Discussion

First, we would like to give a physical interpretation to the above three regions of qualitatively different behavior of stiffness, in particular to the characteristic values $H = 0$ and $H = 2$ separating the three regions. As the qualitative behavior of the exponent α is identical in one- and three-dimensional cases, it is reasonable to discuss the physical nature of the identified regions for one-dimensional systems. It will be seen later, that the interpretation does not depend on the dimensionality of the system. The one-dimensional rough profiles used for simulations presented in Fig. 1, were produced according to the rule

$$h(x) = \sum_q B_{1D}(q) \exp(i(qx + \phi(q))) \quad (9)$$

with

$$B_{1D}(q) = \sqrt{\frac{2\pi}{L} C_{1D}(q)} = \bar{B}_{1D}(-q), \quad (10)$$

random phases $\phi(q) = -\phi(-q)$ on the interval $[0, 2\pi)$ and the one-dimensional power spectrum

$$C_{1D}(q) = Kq^{-2H-1}. \quad (11)$$

The minimum wave number in the sum (9) is $q_{\min} = 2\pi/L$, L is the system size.

We now introduce the notion of roughness of different scales in the following way. Starting with q_{\min} , we can carry out the summation in (9) over exponentially increasing intervals $\{q\}_n = [q_n, q_{n+1})$ with

$$q_n = q_{\min} \cdot e^n, \quad (12)$$

The result of the integration over the n -th interval, we will call “roughness at the n -th scale”. The rms roughness corresponding to the n -th scale is equal to

$$h_n^2 = 2 \int_{q_n}^{q_{n+1}} C_{1D}(q) dq = \frac{K}{H} q_{\min}^{-2H} e^{-2nH} (1 - e^{-2H}). \quad (13)$$

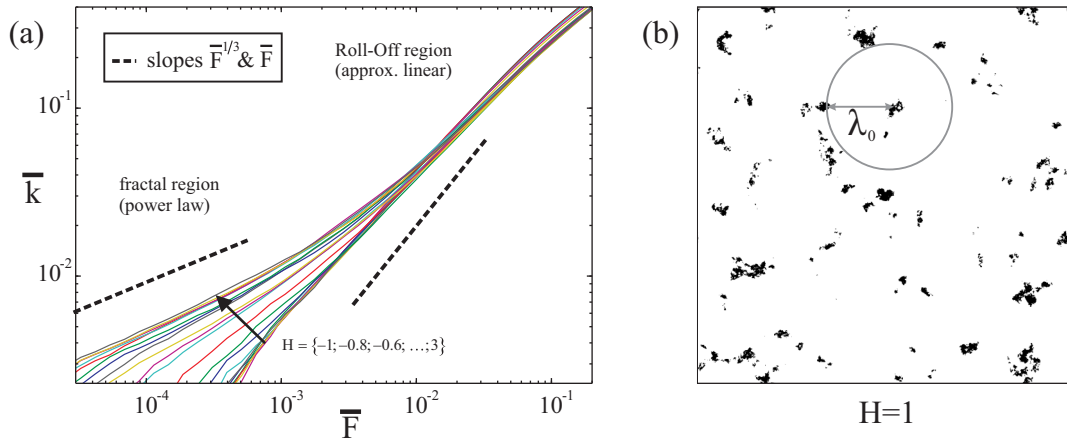


Figure 2 | (a) Dependency of the normal contact stiffness on the normal force at nominally flat surfaces, e.g fractal rough surfaces with long-wavelength roll-off. The colored lines indicate the average of 60 surface samples for each Hurst exponent in the range $-1 \leq H \leq 3$, following the arrow. At low loads, the curves follow eq. (3) with the minimum slope given by $\alpha = 1/3$, see Fig. 1. At higher forces, all curves collapse into an almost linear relation (4). Results obtained by 3D BEM calculations, grid 1024×1024 , lower roll-off at $(q_0L/2\pi) = 6$. (b) Representative contact configuration of an indentation in the region of the linear regime, $H = 1$.

Depending on the parameter H , different relations between roughness of scales with increasing number n are possible.

For $H < 0$, the rms roughness at each smaller scale (corresponding to smaller wave length or to larger wave vectors) is larger than that of the preceding scale: $h_{n+1} > h_n$. This means that the roughness of the smallest scale (largest wave number) dominates the contact behavior. For the force at which the roughness of the smallest scale will be flattened out completely, almost complete contact will be achieved. For much lower forces, the surface will thus act as a large number of independent asperities giving rise to an approximately linear dependence of the stiffness on the normal force (the GW type behavior).

For $H > 2$, the rms curvature of each smaller scale is smaller than that of the preceding larger scale: $h_{n+1}q_{n+1}^2 < h_nq_n^2$. This means that each global peak will have no further local maxima and minima: the whole system will act as only one single asperity, thus leading to the classical result of Hertz¹⁵: $\alpha = 1/3$.

As the replacement of a surface with the power spectrum (1) by a line with the power spectrum (11) leaves the relations of the rms roughness and rms curvatures at different scales invariant, the above arguments are equally applicable to the three-dimensional systems.

In the intermediate region with $0 < H < 2$ there will be always some scales (up to n), at which the roughness is flattened out completely while this is not the case on larger scales (as shown with line d_3 in Fig. 3. In this case, the system acts as only one single asperity of the scale $n - 1$ with the indentation depth corresponding to the roughness of the previous scale. Applying the Hertz theory, this gives the following estimation for the normal force

$$F = \frac{4}{3} E^* R_{n-1}^{1/2} h_n^{3/2} \propto q_n^{-1-H} \tag{14}$$

and for the normal stiffness

$$k = 2E^* R_{n-1}^{1/2} h_n^{1/2} \propto q_n^{-1} \tag{15}$$

where $R_n = (h_n q_n^2)^{-1}$ is the order of magnitude of the radius of curvature at the n -th scale. Determining q_n from (14) and substituting in (15) gives $k \propto F^{1/(H+1)}$. This direct derivation from the 1D line topography thus leads to the same result as the geometrical 3D derivation given in^{13,14}.

Let us now discuss the left hand region $H < 0$ in Fig. 1. In this region, the power α practically does not depend on the parameter H . We will, however, show that it shows a weak dependence on the grid

size or on the number of modes used for the generation of the rough surface.

It can be easily seen that the contact stiffness is closely related to the height distribution of the profile. Often, some standard distribution is assumed, e.g. an exponential one or a Gaussian distribution. We will show that the real distribution of heights is neither of both and that it depends on the number of modes. Let $\Phi(z)$ be the probability density of the heights of the profile, starting with the highest point. In MDR, every spring element has to be indented independently, so the normal force is expressed as

$$F \propto \int_0^d \Phi(z)(d-z) dz. \tag{16}$$

Assuming a power-law function $\Phi(z) \propto z^\beta$, we obtain for the force

$$F \propto \int_0^d z^\beta (d-z) dz \propto d^{\beta+2} \tag{17}$$

and for the stiffness $k = \partial F / \partial d \propto d^{\beta+1}$. Thus, the dependence of the stiffness on the normal force is given by $k \propto F^{(\beta+1)/(\beta+2)}$. We therefore come to the relation

$$\alpha = \frac{\beta + 1}{\beta + 2}. \tag{18}$$

We will now show how to determine β from the number of modes of the rough line that is generated in the 1D case with the help of (9). The summation is carried out over $N = 2^m$ harmonics. Let us first consider a single harmonic, as shown in Fig. 4 (a). In the vicinity of an extremum, the sine function can be approximated as

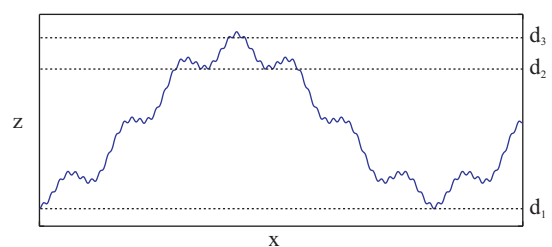


Figure 3 | Example of a rough line with 3 scales. $H = 0.9$.

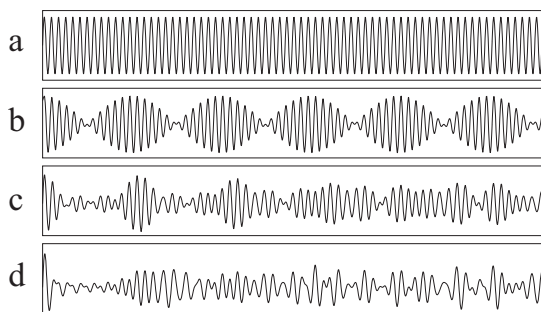


Figure 4 | Different numbers of superposed sine waves. (a) one single sine wave. (b) two sine waves with close frequencies result in a beat wave. (c) beat wave of the 2nd kind using 4 modes. (d) beat wave of the 3rd kind using 8 modes.

$$z(x) \propto x^2. \quad (19)$$

(Note that the z-axis starts at the maximum and shows downward). The corresponding height distribution is equal to

$$\Phi_1(z) = \frac{dN}{dz} = \frac{1}{\Delta x} \frac{1}{f'(x)} \propto x^{-1} \propto z^{-1/2}. \quad (20)$$

A superposition of two waves with similar wave number will produce beats as shown in Fig. 4 (b). In the vicinity of a global maximum, this is a series of parabolic extrema positioned along one parabolic curve of another scale. The resulting height distribution of the whole system is readily determined by the integration

$$\Phi_2(z) \propto \int_0^z (z-z')^{-1/2} z'^{-1/2} dz' = \int_0^1 (1-\xi)^{-1/2} \xi^{-1/2} d\xi = \pi \quad (21)$$

resulting in a constant height probability density. Similarly, four modes will generate a modulated beat wave (beat wave of the 2nd kind, see Fig. 4 (c)) with the height distribution

$$\Phi_3(z) \propto \int_0^z \text{const} \cdot z'^{-1/2} dz' \propto z^{1/2}. \quad (22)$$

It can be seen that increasing the number of modes by the factor of 2 increases the power of the height distribution by 1/2 thus leading to the final equation

$$\beta = -\frac{1}{2} + \frac{1}{2} \log_2(N). \quad (23)$$

With the power α from eq. (18), we get

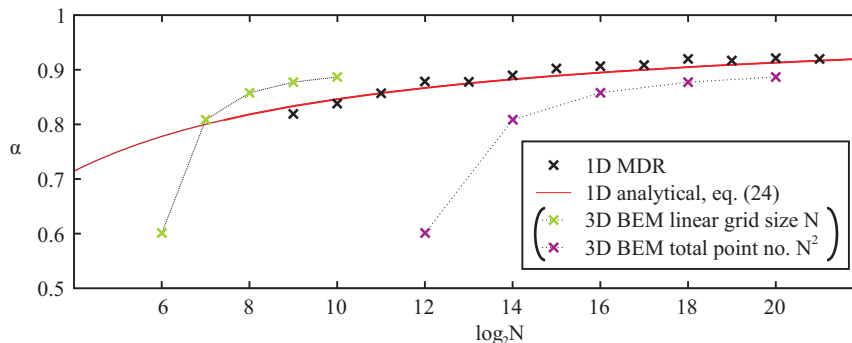


Figure 5 | Numerically observed dependency of the exponent α in eq. (3) for $H < 0$ on the grid size N . See the limiting left hand side of Fig. 1 for reference. Black crosses show the dependency for the 1D analysis. The red line is according to eq. (24). With the 3D BEM and one data set, both interpretations of N are shown with colored crosses. For example, a grid of 1024×1024 can be seen as 2^{10} lines (green cross) or 2^{20} total grid points (purple cross).

$$\alpha = \frac{\beta + 1}{\beta + 2} = \frac{1 + \log_2(N)}{3 + \log_2(N)}. \quad (24)$$

For this result to be valid, the amplitudes of the summed waves must not differ too much, as can be seen from the 2nd step already. However, exact equality is not needed: the beat wave's behavior near the maximum is not altered when two sine waves are added with different but close amplitudes. For this reason, (24) is valid not only for $H = 0$, but also for smaller values of fractal rough surfaces. Fig. 5 shows the numerically determined values of α in comparison with eq. (24). In the case of MDR, the results coincide very well. In 3D, the numerical dependency seems to be similar, but we cannot present an equivalent derivation at this point.

We have seen that the exact value of α for $H < 0$ depends on the number of modes used in simulation. This derivation is valid for any surface spectrum that does not decay too rapidly with increasing wave vector. In particular, this is true for nominally flat surfaces, so it is sensible to discuss the findings of Fig. 2 in this context as well. The surfaces treated there exhibit a roll-off at $q_0 = 6 \cdot (2\pi/L)$, so the corresponding wavelength was 1/6 of the system-size. Therefore, the surface topography shows multiple local maxima as illustrated in Fig. 2b. When brought into contact, only the highest asperity touches at first, resulting in a dependence according to (3). At higher forces, the normal force is carried by multiple local maxima and the dependency becomes almost linear. This result is in agreement with¹⁶, where a linear relation is identified under the condition that “there is a statistical ensemble of high peaks in contact”.

In [21, Chapter 10], the provenance of the linear region is explained by tracing it back to the Greenwood-Williamson case. The basic idea is the following: A nominally flat surface, whose characteristic roughness wavelength λ_0 is considerably shorter than the system-size L , will have multiple local maxima with a characteristic distance of λ_0 . When considering small forces with multiple contact zones resulting from these local maxima, elastic coupling must be included for all points that interact within one zone of contact. In contrast, while these zones are still small compared to λ_0 , it is reasonable to say that the interactions in between local maxima may be neglected. Fig. 2 (b) shows a typical configuration of contact spots. The roll-off wavelength $\lambda_0 = L/6$ is indeed a characteristic distance between the particular spots. Note that this simulation took into account all elastic couplings, including those between distant contact spots.

In the original GW-model, the independent single asperities behave in a Hertzian fashion:

$$\frac{k}{E^*} = \left(6R \frac{F}{E^*}\right)^{1/3} \propto F^{1/3} \quad (25)$$

Thus for a single Hertzian indenter, the force depends on the indentation depth in the following manner

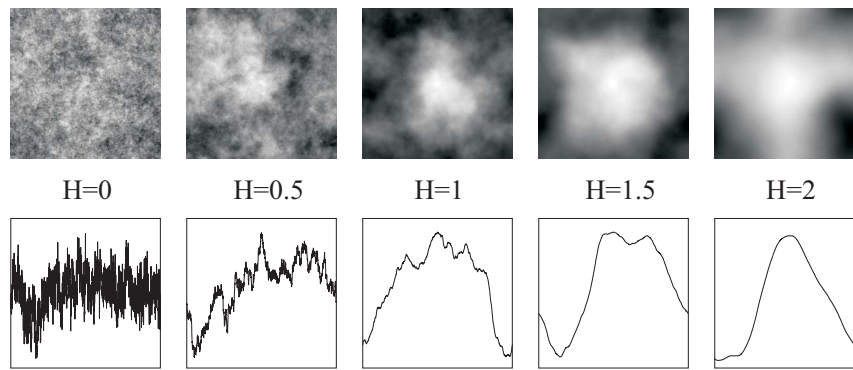


Figure 6 | Samples of randomly rough surfaces with different Hurst Exponent H . The upper images show gray-scale plots of 3D surfaces. Below, corresponding rough lines are shown having the same self-similarity as their 3D counterpart. These lines can be seen as characteristic cuts through the surfaces. All surfaces and lines have been generated using the inverse Fast Fourier Transform. The samples shown here do not include a cut-off or roll-off.

$$F_{Hertz}(d) \propto d^{3/2}. \quad (26)$$

Of course the relation includes elastic coupling within the asperity contact. With the Pohrt/Popov-law (6), we find for a single fractal indenter

$$F_{PP}(d) \propto d^{\frac{H+1}{H}} \quad (27)$$

In the GW model, the linear force-stiffness relation is obtained by assuming an exponential height distribution of the local top peaks and by integrating the forces for all asperities that have come into contact. For the result to be linear, the power in (3) does not need to be $2/3$, the final result of $k \propto F$ does not depend on this power²¹.

These results can be linked back to Fig. 1. Indeed the power spectrum with roll-off is assumed to be constant for any $q < q_0$. The power spectrum being constant corresponds to $C_{2D} \propto q^0$ and thus $H = -1$. For surfaces with roll-off we thus naturally assume the power α in the vicinity of 1. However, we predict a weak dependency of the exact value on the smallest-scale corrugations. This may explain the scattering of the exponent α which can be found in the literature in both numerical and experimental works. In particular, large-scale simulations of nominally flat surfaces conducted in the past suggested $\alpha \approx 1$, see¹⁷. Initially this was seen as a contradiction to the findings of the authors. In fact Fig. 5 reveals that the better the grid resolution of a numerical investigation, the closer the dependence is to a linear law for nominally flat surfaces.

In the current theoretical investigation, all deformations were assumed to be elastic. When considering the contact stiffness and related quantities, this is no major drawback as soon as $0 < H < 1$. Indeed, the contact stress at any particular scale has the order of magnitude $\sigma \approx E^* \langle \nabla z \rangle / 2$, where $\langle \nabla z \rangle$ is the rms surface gradient corresponding to this scale⁵. For $H < 1$, the rms value of surface roughness $\nabla z \propto (\int q^{-2H-2} q^3 dq)^{1/2}$ diverges at the upper integration limit. The surface gradient thus is primarily determined by roughness with the shortest wave length and the breakdown of the elastic behavior occurs at the smallest scales corresponding to the largest rms slope. In contrast, the contact stiffness is determined by the largest wavelength in the power spectrum of the surface roughness, up to the macroscopic size of the current contact spot. It is thus dominated by the long wavelength part of the spectrum and is not sensible to the occurrence at the microscopic scale.

Methods

BEM calculations. The 3D Boundary element method was used to solve the dry contact problem. For a given normal force, the apparent area of contact must be partitioned into two sections. Points that are considered to be in contact must all be deflected to the same height and have positive pressure. All other points are considered not to be in contact, so they must satisfy the condition of zero pressure and a positive gap width to the constant plane of those points that are in contact. Finding

the correct partitioning and redistributing the load within the contact region is done with iterative steps. We used the CG-approach proposed by Polonsky and Keer¹⁸, while for smooth surfaces the local-relaxation approach by Venner and Lubrecht¹⁹ may be more suitable. All discrete grid points influence each other via the elastic coupling, a discrete formulation of the Boussinesq formula for the indentation of an elastic half-space. For this reason, the BEM needs to deal with full (not sparse) matrices, causing the calculations to be costly.

Once the contact problem for a given value of the normal force is solved, the pressure distribution and the resulting deflections are known. The contact stiffness is then determined by taking the resulting partitioning and this time solving the pressures necessary to deflect all contact-points by a constant distance Δd . The effective stiffness can be deduced from the resulting force ΔF as $k = \Delta F / \Delta d$. This last step can be done independently from the actual rough-surface-problem, as the contact stiffness only depends on the specific partitioning, but not on the surface topography or pressure distribution.

We generated surfaces with Hurst exponents from -1 to 3 using the inverse Fourier transform. In the range $0 < H < 2$, surfaces with power spectrum (1) have the property of self-affinity with the Hurst Exponent H . Fig. 6 shows some numerically generated samples of self-affine surfaces in a grayscale plot as well as corresponding self-affine lines, which can be interpreted as characteristic cuts through the 3D surfaces. For these surfaces we solved the contact problem for a wide range of normal forces F_N and determined the resulting contact stiffness. The 3D simulations have been carried out with free boundary conditions outside the apparent contact region and averaging over 60 realizations for every value of H .

1D MDR calculation. The method of dimensionality reduction is a numerical tool for solving contact problems. It has been described in detail in a recent review paper²⁰ as well as in the monograph²¹. Starting from the power-spectrum of a three-dimensional surface, a rough line is generated using

$$C_{1D}(q) = \pi q C_{2D}(q), \quad (28)$$

In the case of fractal surfaces we obtain

$$C_{1D}(q) \propto q^{-2H-1} \quad (29)$$

Again, fractal rough lines have been generated using the inverse Fourier transform with random phases. As in the 3D case, we considered spectra with no roll-off or cut-off. Instead, eq. (29) was valid all the way from the system size L down to the grid spacing $\Delta x = L/N$. Random samples of these rough lines can be found in Fig. 6. The newly generated lines also include the self-similar property with the same Hurst exponent as their 3D counterparts, so these samples can be considered characteristic cuts through the equivalent 3D surfaces.

In the MDR the discrete elements of the rough line are independent, so the complexity of the numerical process is linear in the total number of line points N . For this reason, all simulations could be done quickly, allowing for parameter studies with high resolution and 500 samples in each case.

1. Popov, V. L. *Contact Mechanics And Friction. Physical Principles And Applications* (Springer-Verlag, Heidelberg, 2010).
2. Bowden, F. P. & Tabor, D. *The Friction And Lubrication Of Solids* (Clarendon Press, Oxford, 1986).
3. Archard, J. F. Elastic deformation and the laws of friction. *Proc. R. Soc. A* **243**, 190 (1957).
4. Greenwood, J. A. & Williamson, J. B. P. Contact of nominally flat surfaces. *Proc. R. Soc. A* **295**, 300 (1966).
5. Hyun, S. & Robbins, M. O. Elastic contact between rough surfaces: effect of roughness at large and small wavelengths. *Tribol. Intern.* **40**, 1413 (2007).



6. Campana, C. & Müser, M. H. Practical Green's function approach to the simulation of elastic semi-infinite solids. *Phys. Rev. B* **74**, 075420 (2006).
7. Akarapu, S., Sharp, T. & Robbins, M. O. Stiffness of contacts between rough surfaces. *Phys. Rev. Lett.* **106**, 204301 (2011).
8. Campana, C., Persson, B. N. J. & Müser, M. H. Transverse and normal interfacial stiffness of solids with randomly rough surfaces. *J. Phys. Cond. Matter.* **23**, 085001 (2011).
9. Barber, J. R. Bounds on the electrical resistance between contacting elastic rough bodies. *Proc R. Soc. Lond. A* **495**, 53–66 (2003).
10. Ciavarella, M., Dibello, S. & Demelio, G. Conductance of rough random profiles. *Int. J. Solids & Structures* **45**, 879–893 (2007).
11. Paggi, M. & Barber, J. Contact conductance of rough surfaces composed of modified RMD patches. *Int. J. of heat and mass transfer* **54**, 4664–8 (2011).
12. Pohrt, R. & Popov, V. L. Normal contact stiffness of elastic solids with fractal rough surfaces. *Phys. Rev. Lett.* **108**, 104301 (2012).
13. Pohrt, R., Popov, V. L. & Filippov, A. E. Investigation of the dry normal contact between fractal rough surfaces using the reduction method, comparison to 3D simulations. *Phys. Rev. E* **86**, 026710 (2012).
14. Pohrt, R. & Popov, V. L. Investigation of the dry normal contact between fractal rough surfaces using the reduction method, comparison to 3D simulations. *Phys. Mesomech.* **15**, 275–279 (2012).
15. Hertz, H. Über die Berührung fester elastischer Körper. *Journal für die reine und angewandte Mathematik* **92**, 156–15 (1881).
16. Pastewka, L., Prodanov, N., Lorenz, B., Müser, M. H., Robbins, M. O. & Persson, B. N. J. Finite-size scaling in the interfacial stiffness of rough elastic contacts. *Phys. Rev. E* **87**, 062809 (2013).
17. Campana, C., Müser, M. H. & Robbins, M. O. Elastic contact between self-affine surfaces: Comparison of numerical stress and contact correlation functions with analytic predictions. *J. Phys.: Condens. Matter* **20**, 355013, 1–12 (2008).
18. Polonsky, I. A. & Keer, L. M. A numerical method for solving rough contact problems based on the multi-level multi-summation and conjugate gradient techniques. *Wear* **231**, 206–210 (1999).
19. Venner, C. H. & Lubrecht, A. A. *Multilevel Methods in Lubrication* (Elsevier, Amsterdam 2000).
20. Popov, V. L. Method of reduction of dimensionality in contact and friction mechanics: A linkage between micro and macro scales. *Friction* **1**, 41–62 (2013).
21. Popov, V. L. & Heß, M. *Methode der Dimensionsreduktion in Kontaktmechanik und Reibung* (Springer-Verlag, Heidelberg, 2013).

Acknowledgments

We acknowledge financial support by the Deutsche Forschungsgemeinschaft (DFG).

Author contributions

R.P. performed the BEM and MDR calculations, both authors (R.P. and V.P.) carried out the analysis and contributed to the writing of the manuscript.

Additional information

Competing financial interests: The authors declare no competing financial interests.

How to cite this article: Pohrt, R. & Popov, V.L. Contact stiffness of randomly rough surfaces. *Sci. Rep.* **3**, 3293; DOI:10.1038/srep03293 (2013).



This work is licensed under a Creative Commons Attribution-NonCommercial-ShareAlike 3.0 Unported license. To view a copy of this license, visit <http://creativecommons.org/licenses/by-nc-sa/3.0>